

# Evolution of size distribution of nascent soot in *n*- and *i*-butanol flames

Joaquin Camacho, Sydnie Lieb, Hai Wang\*

Department of Aerospace and Mechanical Engineering, University of Southern California, Los Angeles,  
CA 90089-1453, USA

Available online 12 July 2012

## Abstract

The impact of fuel bound oxygen on the sooting behavior of butanol fuels was examined by following the evolution of the particle size distribution function (PSDF) of nascent soot produced in atmospheric pressure burner stabilized stagnation (BSS) flames of *n*-butanol and *i*-butanol. Similar experiments were carried out for *i*-butane and *n*-butane flames to better understand the influence of fuel structure and the presence of the alcohol group on detailed processes of soot nucleation and growth. In terms of fuel structure, the branched chain functionality has the most observable effect on soot formation. The onset of soot nucleation is faster in the branched fuels in comparison to the straight-chain counterparts. Under the same C/O ratio, however, the butanol flames were found to nucleate soot earlier and have higher soot volume fraction than the butane flames. A combustion reaction model for *i*-butanol and *n*-butanol was used to explore the precursor chemistry. Similar to the measured PSDF, benzene is computed to rise earlier in flames of the branched fuels than the straight-chain fuels.

© 2012 The Combustion Institute. Published by Elsevier Inc. All rights reserved.

**Keywords:** Premixed flame; Soot; Particle size distribution; Kinetics

## 1. Introduction

Soot formation is a kinetic process of combustion [1] that is integral to the optimization of any combustion device. Understanding the processes of soot formation in butanols – a potential source of fuels derived from biomass conversion [2–4], and how these processes vary with fuel structures will be critical to rational utilization of these biofuels. Also, the examination of oxygenated fuels may reveal insights into mechanisms of soot nucleation and growth for all fuels in general. Fundamental combustion properties such as laminar flame speeds and ignition delay times have been deter-

mined and flow reactor measurements have been carried out to describe the kinetic behavior of *i*-butanol and *n*-butanol fuels over a wide range of conditions [5–19]. Measurements of detailed flame structures have been made in low-pressure, burner stabilized flames of butanol isomers using photo-ionization mass spectrometry [20–22]. Coflow diffusion flames doped with butanols have been studied [23,24]. Much of the experimental work conducted thus far has been used to support the recent extensive development of flame chemistry for the butanol isomers (see, e.g., [5,10–14,16,17,22,25,26]).

Global sooting behavior of butane isomers has been studied in diffusion flames [27,28], but a cross comparison of the behaviors of the fuel structures, including the isomeric effect and the role of alcohol group on the nucleation and growth of

\* Corresponding author. Fax: +1 213 740 8071.  
E-mail address: [haiw@usc.edu](mailto:haiw@usc.edu) (H. Wang).

nascent soot has not been made. Development of soot chemistry requires more direct observations of sooting behavior because the nucleation and growth of soot is often dictated by competing kinetic processes [1]. One such competition originates from the fuel structure itself. In recent studies of intermediate species formed in low-pressure burner stabilized fuel-rich flames, Oßwald et al. [21] found a drastic sensitivity for the production of various intermediate species with respect to the fuel structure. In particular, *tert*-butanol and *i*-butanol flames yield significantly more aromatic species than in *n*- or 2-butanol flames. This effect is expected to propagate into soot nucleation and growth in butanol flames.

In the present study, the role of fuel structure and oxygenation on soot formation was investigated in a set of laminar premixed flames of *n*-butane, *i*-butane, *n*-butanol and *i*-butanol. The emphasis of the study was placed on probing the evolution of the detailed particle size distribution function (PSDF). Cross comparisons were made with respect to butanol isomeric branching structure and between butanols and their parent hydrocarbon analogs. A systematic approach was taken such that the effect of local flame temperature and carbon to oxygen ratio are isolated from the fuel structure effect.

The burner stabilized stagnation (BSS) flame approach coupled with mobility sizing; described in detail elsewhere [29,30] was employed to investigate the evolution of PSDFs in nascent soot from particle nucleation to mass growth. The method is inherently intrusive to flame but our technique accounts for flame perturbation by the probe explicitly by treating it, experimentally and computationally, as the downstream boundary of the flame. With the flow field defined, the flame temperature and species concentrations can be directly modeled using a quasi one dimensional code without imposing a measured temperature profile or correcting for artificial probe perturbation [29]. A similar method without the use of a flow stagnation surface has been used by us earlier [31–34] and by other groups (see, e.g., [35–38]).

To obtain reliable radiation correction for the measured temperature and to explore the fundamental kinetic causes for the fuel structure effects, a high temperature *n*- and *i*-butanol combustion model is used for numerical simulations. The model combines *n*- and *i*-butanol chemistry of Moss et al. [5] with existing C<sub>1</sub>–C<sub>4</sub> combustion chemistry in USC Mech II [39]. In this way, the butane and butanol chemistry is made consistent to each other for computation of the temperature profiles of the flames studied. Additionally, analysis of the concentration profiles computed for benzene and other gas-phase species was made as such an analysis provides insights into soot nucleation and formation [40].

## 2. Experimental

The BSS flame approach [29,30] was employed to probe nascent soot formation in butane and butanol flames. The BSS flame configuration can be simulated directly as a quasi one-dimensional problem because the stagnation surface acts as the sampling probe and flame boundary condition simultaneously. One lightly sooting flame was stabilized for each fuel considered at atmospheric pressure with nearly equal maximum flame temperature and flow conditions. Furthermore, the total C/O ratio of the flames was held fixed. The conditions of the flames are summarized in Table 1. The gas temperature profiles were measured with a Y<sub>2</sub>O<sub>3</sub>/BeO coated type-S thermocouple with radiation correction using a procedure discussed earlier [41]. The bead diameter was around 0.3 mm after coating.

The flat flame burner is 5 cm in diameter and is uncooled because of potential condensation of the fuel in the porous material. Without water cooling, however, the pores tend to close in its center, thus modifying the local unburned gas velocity. For this reason, fresh porous material was always used to keep the flame roughly one dimensional. A sheath of nitrogen shields the flame to prevent radial entrainment and diffusion of oxygen from ambient air. Liquid *n*-butanol and *i*-butanol, both acquired from Sigma–Aldrich (ACS Reagent grade, 99% purity) were vaporized and injected into the fuel line in a manner similar to a previous study [30]. The mass flow rates of *n*-butane, *i*-butane, oxygen, argon and nitrogen were measured by critical orifices and the flow of argon driving the fuel nebulizer was calibrated by a bubble meter. The butane isomers were C.P. grade, purchased from Gilmore gas.

Particle size distributions were determined with a TSI 3080 SMPS using a sample dilution technique developed earlier and improved over time [31–34,41,42]. The sample gas entered the probe through an orifice and was immediately diluted with a cold nitrogen flow to prevent particle losses. The dilution range and calibration has been used before and care was taken to avoid diffusion losses, condensation of higher-molecular weight hydrocarbons, and probe-induced particle–particle coagulation during dilution [29]. Limitations of the Cunningham slip correction cause particles below 10 nm to be overestimated by mobility measurements and thus a nanoparticle transport theory was used for small particles to obtain more accurate particles sizes [43–45].

The experimentally measured temperature profiles are radiation corrected by using transport and flow properties that are calculated by a modified version of OPPDIF [46]. The ratio of the burner-to-probe separation to the burner diameter is much less than unity so the quasi one-dimensional assumption applies. The flame chemistry was

Table 1  
Summary of flame conditions.

Mole fractions <sup>a</sup>			Equivalence ratio, $\phi$	Velocity <sup>b</sup> , $v_0$ (cm/s)	Maximum temperature, $T_{f,max}$ (K)	
Fuel	O <sub>2</sub>	C/O				
<i>n</i> -C <sub>4</sub> H <sub>9</sub> OH	0.109	0.290	0.632	2.25	4.64	1790 ± 70
<i>i</i> -C <sub>4</sub> H <sub>9</sub> OH	0.109	0.290	0.632	2.25	4.64	1790 ± 70
<i>n</i> -C <sub>4</sub> H <sub>10</sub>	0.0958	0.304	0.630	2.05	3.58	1750 ± 70
<i>i</i> -C <sub>4</sub> H <sub>10</sub>	0.0958	0.304	0.630	2.05	3.58	1790 ± 70

<sup>a</sup> The balance gas is argon.

<sup>b</sup> STP cold gas velocity.

calculated with USC Mech II [39] for the butane isomers. A butanol combustion model will be introduced below and used for simulation of the butanol flames. By energy conservation, the modified OPPIF code allows for the calculation of the temperature and species profile without the need for a measured temperature profile as an input. The radiation corrected temperature profiles are compared to the calculated OPPDIF profile to test the validity of the experimental and numerical procedures. The temperature closest to the burner surface that can be measured is equal to one half of the thermocouple bead diameter (0.15 mm). The inlet temperature was extrapolated from the measured temperature profile immediately adjacent to the burner surface. The temperature variation is roughly linear with respect to the distance, as one would expect because in that region the dominant heat transfer mechanism is heat conduction. The probe temperature was measured with a type K thermocouple embedded on the stagnation surface.

The chemistry for high-temperature oxidation of the butanol isomers is extracted from Moss et al. [5] and superimposed over USC Mech II [39]. The two models were first combined by Veloo et al. [47] to model the laminar flame speed of *n*-butanol flames. The current work added additional chemistry of *i*-butanol. This subset of the model is, again, based on Ref. [5]. This approach ensures consistency when the flame chemistry of butanols is compared to their parent non-oxygenated hydrocarbon fuels, although the prediction accuracy of high-molecular weight species for all fuels tested has not been directly verified under the conditions tested. The combination of the two models was also motivated by the consideration that USC Mech II includes an adequate amount of fuel-rich chemistry leading to aromatics formation from small molecular fragments. The resulting model, comprised of 959 reactions and 136 species, is used here primarily for correction of radiative heat loss and should not be viewed or used as an independently proposed model for butanol combustion beyond the current purpose. The reaction mechanism, and thermochemical and transport databases are available in the Supplemental data.

### 3. Results and discussion

To ensure an accurate prediction of the heat release rate in the BSS flames, the reaction model was first subject to validation against the laminar flame speed previously reported for *n*- and *i*-butanol-air mixtures at an unburned mixture temperature of 343 K [7,8]. The comparison between the measured and calculated *n*-butanol flame speed is shown in Fig. 1. It is seen that the combined model predicts the flame speed rather well.

Local temperature is the dominant parameter which governs the soot chemistry. A comparison between the measured/radiation corrected and simulated temperature profiles is shown in Fig. 2 for the two butanol isomers at a series of burner-to-stagnation surface separation distances. The degree to which the stagnation probe causes heat loss is shown. In both fuels, the agreement between radiation corrected measurements and simulated temperatures is within thermocouple positioning uncertainty ( $\pm 0.03$  cm) and the temperature measurement uncertainty ( $\pm 70$  K around the peak temperature region). As we discussed in Ref. [41], literature emissivity values for Y/Be/O coating are between 0.3 and 0.6 [48,49]. The radiation-corrected temperature was estimated to be the average of the two limiting cases which also yielded the uncertainty bounds for the temperature shown in the figure.

The model solves the energy equation without the measured temperature profiles as an input. Thus, agreement between radiation corrected measurements and the simulation addresses uncertainty within the mechanism itself by yielding information on local heat release and loss rates [29]. Such information allows for the uncertainty within the simulated local temperature to be defined along with the resulting Arrhenius reaction kinetics and species transport. Furthermore, the agreement in measured temperatures and the model confirms that the flame conditions are nearly identical across all the flames studied.

A similar plot for the measured and simulated temperature profiles is shown in Fig. 3 for the *n*- and *i*-butane flames. These temperature profiles are very similar to those in the butanol flames. The only exception is for the *n*-butane flame which

gives a maximum flame temperature of 1750 K, rather than 1790 K measured in other flames. The cause for the difference is the heat release rate. Under comparable conditions, *n*-butane flames tend to have a slightly higher flame speed, leading to a faster temperature rise in the preflame region. The increase in the temperature gradient causes an increased heat loss into the burner; and the maximum flame temperature is reduced accordingly.

The PSDFs for sooting flames were measured for the butane and butanol isomers. The evolution of the PSDF from nucleation of soot to its growth for the two butanol isomers is summarized in Fig. 4. The evolution of the PSDFs is similar to previous measurements of ethylene and dodecane under comparable flame conditions [29,30]. At the early stage of soot formation, newly nucleated particles burst into the lower end of the measurable size window at 2.4 nm. These particles grow in size, producing a shoulder in the PSDF, which grows into a log-normal distribution at larger burner-to-stagnation surface separations. Meanwhile, nucleation persists well into the large separation distances with the PSDF characterized by a strong tail throughout the particle size growth period.

Overall, the competition between nucleation and growth appears to be similar across the two butanol flames, with the differences being only quantitative and subtle. As Fig. 4 shows, the onset of nucleation is slightly delayed in the *n*-butanol flame compared to the *i*-butanol flame, but during the mass and size growth stages, and PSDFs become less distinguishable. At the largest separation distances probed ( $H_p = 1.2$  and 1.4 cm), the lognormal part of the distribution nearly overlaps each other, whereas the PSDF tails exhibit reproducible and subtle differences between the two flames.

Detailed behaviors of nascent soot formation in all four flames probed are by all means similar. Figure 5 provides a comparison of the PSDFs at three separation distances. The three positions represent three separate stages of sooting processes. The distributions at  $H_p = 0.8$  cm is indicative of particle nucleation; those at 1.0 cm show the onset of primary particle formation; and the PSDFs at 1.4 cm illustrate the lognormal nature of the primary particle size distribution with median diameters around 30 nm. Overall, the differences among the four flames probed are only in the quantitative aspects of the PSDF and its evolution.

The global sooting behavior for each flame can be determined in terms of the total soot volume fraction by integrating the PSDF over all particle sizes measured ( $>2.5$  nm). Obviously, particles smaller than the lower detection limit of the particle size do not contribute to volume fraction substantially. The soot volume fraction as a function of burner to probe separation,  $H_p$ , is shown in Fig. 6. At the same C/O ratio, the butanol fuels have higher volume fraction than the alkane fuels

throughout the flame. In addition, Fig. 4 shows that the branched alcohol and branched alkane have greater volume fractions relative to their straight chain counterparts. These observations are consistent with previous measurements for sooting tendency of the butanol fuels in doped co-flow diffusion flames [23,24]. In those studies, it was determined that the degree of branching within the fuel structure and the fuel carbon number controls the sooting behavior rather than the fuel bound oxygen.

*i*-Butanol and *i*-butane also show faster onset of nucleation than their straight chain counterparts. The difference in the nucleation rate is exhibited in the onset of volume fraction rise. Beyond the nucleation stage, the mass growth rates also differ. The difference may be assessed by an arbitrary shift of the volume fraction profiles spatially to match the nucleation part of the curve for *i*-butanol, as shown in the inset of Fig. 6. Clearly, the fuel giving rise to faster particle nucleation also yields faster size and mass growth rates. The final difference in the volume fraction is close to an order of magnitude between the sootiest *i*-butanol flame and the least sooty *n*-butane flame. As shown in Table 1, the cold gas velocity of the two butane flames is smaller than that of the butanol flames. At the same separation distance, the particle residence time in the butane flames is longer than that in the butanol flames. Hence, the observed differences in the nucleation and mass growth rates cannot be attributed to the difference in the reaction time.

The higher volume of soot measured for the alcohol flames can be attributed, to a large extent, to the higher equivalence ratio than those of the butane flames. Under the same C/O ratio, however, our results indicate that alcohols do not always yield less soot to their alkane counterparts. Additional tests not shown here indicate that the butane flames are as sooty as the butanol flames if the equivalence ratio is made equal. In any case, any effect of the fuel bound oxygen on soot forma-

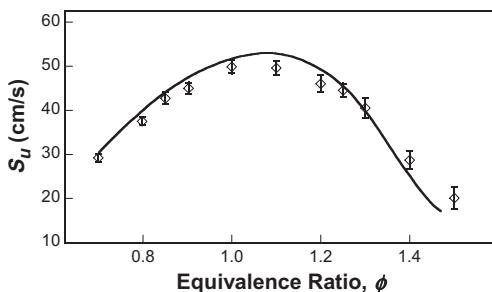


Fig. 1. Comparison of predicted and measured flame speeds ( $S_u$ ) of *n*-butanol/air flames at 1 atm and an unburned gas temperature of 343 K. The data are taken from [7].

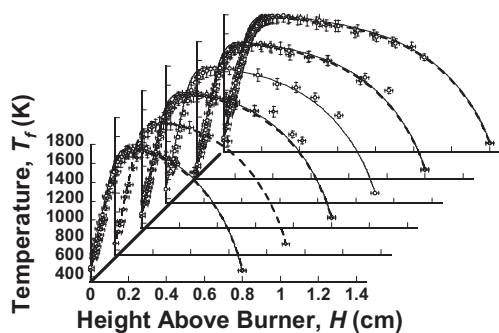


Fig. 2. Measured (symbols) and simulated (lines) temperature profiles. Open symbols and solid lines: *i*-butanol; filled symbols and dashed lines: *n*-butanol. The vertical error bars represent the limiting emissivity of 0.3 and 0.6 (see text).

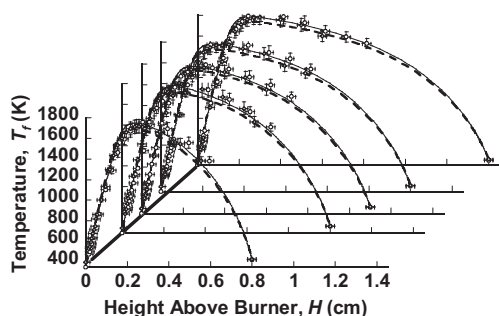


Fig. 3. Measured (symbols) and simulated (lines) temperature profiles. Open symbols and solid lines: *i*-butane; filled symbols and dashed lines: *n*-butane. The vertical error bars represent the limiting emissivity of 0.3 and 0.6 (see text).

tion is overshadowed by the effect of the branched chain within the fuel structure.

For the fuels studied the most conclusive observation of sooting behavior results from the straight versus branched chain within the fuel structure. Soot precursors calculated from the flame chemistry were examined to better understand the quantitative difference in soot formation among the four flames. The model presented does not extend to a fundamental description of soot nucleation and growth. However, the sensitivity of soot precursor formation to the fuel structure can be evaluated.

Species profiles and reaction rates were analyzed numerically for the BSS flames. In particular, the formation of benzene was analyzed to gain insight into the impact of the fuel bound oxygen and branched chains on soot formation. The species mole fraction profile calculated for benzene at several  $H_p$  is shown in Fig. 7 for the fuels studied. At the nucleation stage ( $H_p = 0.80$  cm), the benzene concentration is predicted to be significantly

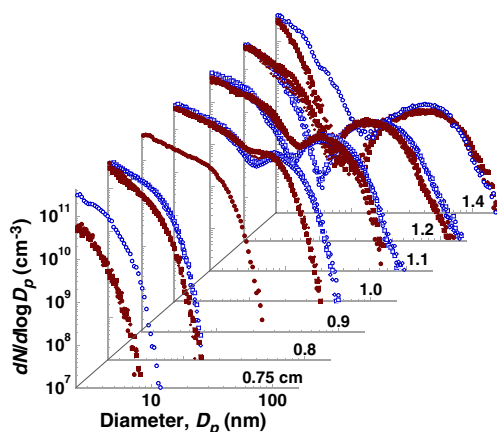


Fig. 4. Measured PSDFs for *i*-butanol (open symbols) and *n*-butanol (filled symbols) flames.

higher in the branched chain fuels than in the straight chain fuels. The benzene concentration of the branched isomers is predicted to be 40% greater than the normal isomers in the post-flame region of the nucleation stage. These results are consistent with the earlier onset of soot nucleation observed in flames burning branched chain fuels. The relative concentration of benzene at the nucleation stage is also in agreement with observations of premixed burner stabilized flames [21] and doped co-flow diffusion flames where the peak benzene concentration ranked as *i*-butane > *i*-butanol > *n*-butane ~ *n*-butanol [23,24].

Formation of the first aromatic ring depends on the formation of acetylene and propargyl radical. The species profile calculated for acetylene and propargyl at several  $H_p$  is shown in Fig. 8. The higher propargyl concentration in the *i*-butanol flame is attributable to a larger propene concentration. At  $H_p = 0.8$  cm, the peak propene concentration is about 3 times larger than the concentration in the *n*-butanol flames. Propene formed serves to increase the concentration of the propargyl radicals which can then recombine to form benzene. In contrast, acetaldehyde and ethyl radical are the most significant intermediate products formed during the initial reactions of *n*-butanol. The above view is consistent with the experimental observations made in low-pressure burner stabilized flames by Oßwald et al. [21]. Comparing the *n*- and *i*-butanol flames they probed by molecular beam synchrotron photoionization mass spectrometry, the peak concentrations of propene, propyne, propargyl and consequently, benzene in the *i*-butanol flame are decidedly higher than those measured for the *n*-butanol flame. Hence, both the previous and current analyses suggest that the observed difference in the sooting behaviors is attributable to the competition of forming  $C_2$  versus  $C_3$  intermediates during initial attack on

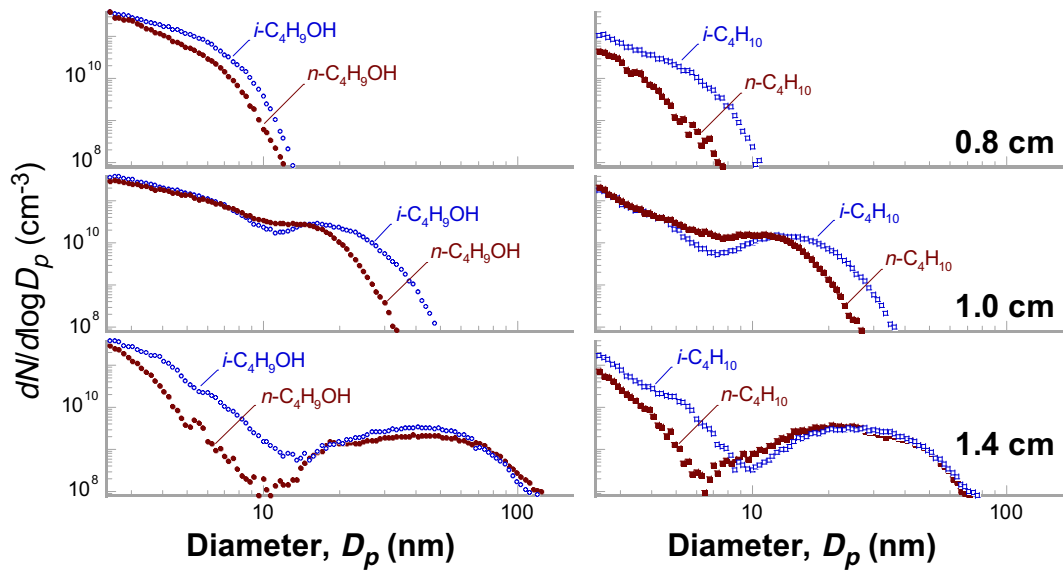


Fig. 5. Comparison of PSDFs for *i*-butanol, *n*-butanol, *i*-butane and *n*-butane flames at selected burner-to-stagnation surface separations.

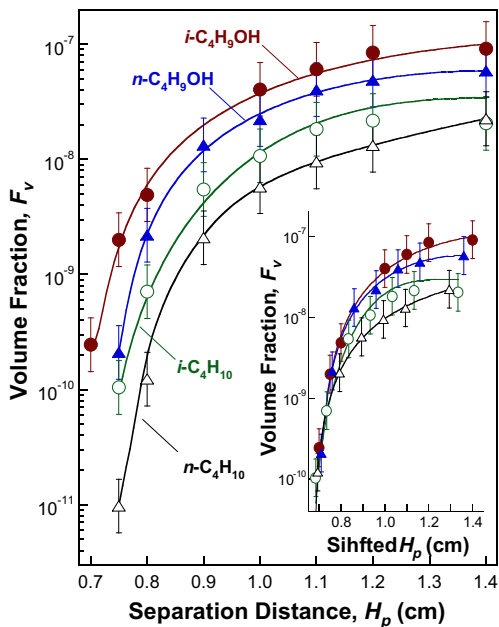


Fig. 6. Volume fraction of nascent soot with  $D_p > 2.4$  nm (symbols) measured at several  $H_p$  for all fuels tested. Lines are drawn to guide the eye. Inset: profiles shifted spatially to illustrate the mass growth rates beyond nucleation.

the fuel, and that *i*-butanol promotes the production of  $C_3$  species and benzene via propene.

Unlike the nucleation stage, the observed sooting behavior at the mass growth stage is not directly

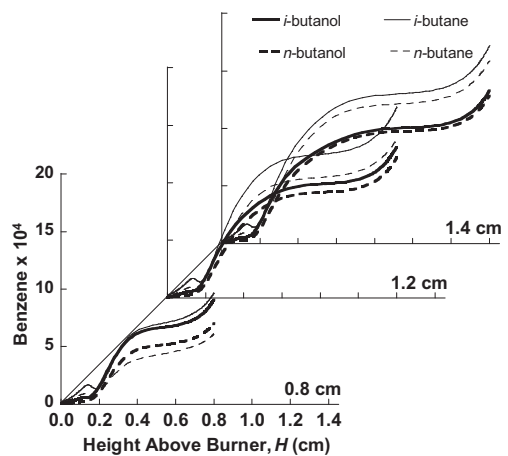


Fig. 7. Mole fraction profiles of benzene computed at several  $H_p$ .

explained by the predicted species profiles of soot precursors. The dependence on fuel structure for both the observed sooting behavior and the predicted benzene concentration becomes less clear at the mass growth stage. The branched fuels have greater benzene formation in the nucleation stage. However, Fig. 7 shows that *n*-butane flames have more significant benzene formation at the mass growth stage ( $H_p = 1.2$  cm). This exchange in position indicates that propargyl recombination becomes competitive in the straight chain fuels towards the later stage of the flame, where the flame

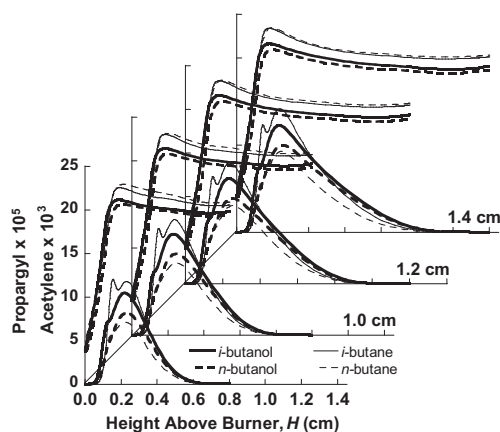


Fig. 8. Mole fraction profiles of  $C_2H_2$  (top) and  $C_3H_3$  (bottom) for computed at several  $H_p$ .

chemistry is more sensitive to the thermodynamic condition rather than the initial fuel structure.

#### 4. Conclusion

The evolution of the PSDF of nascent soot was examined in *n*-butanol, *i*-butanol, *n*-butane and *i*-butane flames to understand the impact of fuel bound oxygen and the fuel structure on the detailed sooting behavior of butanol fuels. The flames were probed under the same C/O ratio and nearly identical temperature. Under the same C/O ratio, butanol flames in fact nucleate soot earlier and gave greater soot volume fractions than the butane flames. In terms of fuel structure, the branched chain functionality has the most observable effect on soot formation. The onset of soot nucleation is faster in the branched fuels in comparison to the straight-chain counterparts. The faster nucleation rate also propagates into the mass growth stage. A combustion reaction model for *i*-butanol and *n*-butanol was applied to analyze the BSS configuration to elucidate the role of soot precursors on the observed sooting behavior. It is shown that for the fuel studied, the fuel structure effect is largely exhibited in the relative importance of  $C_2$  versus  $C_3$  intermediate species formed during the initial stage of fuel breakdown.

#### Acknowledgements

The authors wish to thank Dr. Peter Veloo for providing a copy of the combined USC Mech II and *n*-butanol reaction model. The work was supported by the Combustion Energy Frontier Research Center (CEFRC), an Energy Frontier Research Center funded by the U.S. Department

of Energy, Office of Science, Office of Basic Energy Sciences under Award Number DE-SC0001198.

#### Appendix A. Supplementary data

Supplementary data associated with this article can be found, in the online version, at <http://dx.doi.org/10.1016/j.proci.2012.05.100>.

#### References

- [1] H. Wang, *Proc. Combust. Inst.* 33 (2011) 41–67.
- [2] S. Atsumi, T. Hanai, J.C. Liao, *Nature* 451 (2008) 86–89.
- [3] J.D. Taylor, M.M. Jenni, M.W. Peters, *Top. Catal.* 53 (2010) 1224–1230.
- [4] P.S. Nigam, A. Singh, *Prog. Energy Combust. Sci.* 37 (2011) 52–68.
- [5] J.T. Moss, A.M. Berkowitz, M.A. Oehlschlaeger, et al., *J. Phys. Chem. A* 112 (2008) 10843–10855.
- [6] S. Vranckx, K.A. Heufer, C. Lee, et al., *Combust. Flame* 158 (2011) 1444–1455.
- [7] P.S. Veloo, Y.L. Wang, F.N. Egolfopoulos, C.K. Westbrook, *Combust. Flame* 157 (2010) 1989–2004.
- [8] P.S. Veloo, F.N. Egolfopoulos, *Proc. Combust. Inst.* 33 (2011) 987–993.
- [9] X.L. Gu, Z.H. Huang, S. Wu, Q.Q. Li, *Combust. Flame* 157 (2010) 2318–2325.
- [10] K.M. Van Geem, S.P. Pyl, G.B. Marin, M.R. Harper, W.H. Green, *Ind. Eng. Chem. Res.* 49 (2010) 10399–10420.
- [11] G. Black, H.J. Curran, S. Pichon, J.M. Simmie, V. Zhukov, *Combust. Flame* 157 (2010) 363–373.
- [12] P. Dagaut, S.M. Sarathy, M.J. Thomson, *Proc. Combust. Inst.* 32 (2009) 229–237.
- [13] C. Togbe, A. Mze, Amir, P. Dagaut, *Energy Fuels* 24 (2010) 5244–5256.
- [14] M.R. Harper, K.M. Van Geem, S.P. Pyl, G.B. Marin, W.H. Green, *Combust. Flame* 158 (2011) 16–41.
- [15] K.E. Noorani, B. Akih-Kumgeh, J.M. Bergthorson, *Energy Fuels* 24 (2011) 5834–5843.
- [16] R. Grana, A. Frassoldati, T. Faravelli, et al., *Combust. Flame* 157 (2011) 2137–2154.
- [17] I. Stranic, D.P. Chase, J.T. Harmon, S. Yang, D.F. Davidson, R.K. Hanson, *Combust. Flame* (2011).
- [18] B.W. Weber, K. Kumar, Y. Zhang, C.-J. Sung, *Combust. Flame* 158 (2011) 809–819.
- [19] D.M.A. Karwat, S.W. Wagnon, P.D. Teini, M.S. Wooldridge, *J. Phys. Chem. A* 115 (2011) 4909–4921.
- [20] B. Yang, P. Obwald, Y. Li, et al., *Combust. Flame* 148 (2007) 198–209.
- [21] P. Obwald, H. Guldenberg, K. Kohse-Höinghaus, B. Yang, T. Yuan, F. Qi, *Combust. Flame* 158 (2011) 2–15.
- [22] N. Hansen, M.R. Harper, W.H. Green, *Phys. Chem. Chem. Phys.* 13 (2011) 20262–20274.
- [23] C.S. McEnally, L.D. Pfeifferle, *Proc. Combust. Inst.* 30 (2005) 1363–1370.
- [24] C.S. McEnally, L.D. Pfeifferle, *Environ. Sci. Technol.* 45 (2011) 2498–2503.

- [25] C.-W. Zhou, J.M. Simmie, H.J. Curran, *Combust. Flame* 158 (2011) 726–731.
- [26] K. Kohse-Höinghaus, P. Obwald, T.A. Cool, et al., *Angew. Chem. Int. Edit.* 49 (2010) 3572–3597.
- [27] S. Trottier, H. Guo, G.J. Smallwood, M.R. Johnson, *Proc. Combust. Inst.* 31 (2007) 611–619.
- [28] A.E. Karatas, M. Commodo, O.L. Gulder, *Energy Fuels* 24 (2011) 4912–4918.
- [29] A.D. Abid, J. Camacho, D.A. Sheen, H. Wang, *Combust. Flame* 156 (2009) 1862–1870.
- [30] A.D. Abid, J. Camacho, D.A. Sheen, H. Wang, *Energy Fuels* 23 (2009) 4286–4294.
- [31] B. Zhao, Z. Yang, M.V. Johnston, et al., *Combust. Flame* 133 (2003) 173–188.
- [32] B. Zhao, Z. Yang, J. Wang, M.V. Johnston, H. Wang, *Aerosol. Sci. Technol.* 37 (2003) 611–620.
- [33] B. Zhao, Z. Yang, Z. Li, M.V. Johnston, H. Wang, H. Richter, *Proc. Combust. Inst.* 30 (2005) 1441–1448.
- [34] B. Zhao, K. Uchikawa, H. Wang, *Proc. Combust. Inst.* 31 (2007) 851–860.
- [35] L.A. Sgro, A. De Filippo, G. Lanzaolo, A. D'Alessio, *Proc. Combust. Inst.* 31 (2007) 631–638.
- [36] L.A. Sgro, A. Borghese, L. Speranza, et al., *Environ. Sci. Technol.* 42 (2008) 859–863.
- [37] L.A. Sgro, A.C. Barone, M. Commodo, et al., *Proc. Combust. Inst.* 32 (2009) 689–696.
- [38] C.A. Echavarria, A.F. Sarofim, J.S. Lighty, A. D'Anna, *Proc. Combust. Inst.* 32 (2009) 705–711.
- [39] H. Wang, X. You, A. V. Joshi, S. G. Davis, A. Laskin, F. N. Egolfopoulos, C. K. Law USC Mech Version II, High-Temperature Combustion Reaction Model of H<sub>2</sub>/CO/C<sub>1</sub>-C<sub>4</sub> Compounds, 2007.
- [40] H. Wang, M. Frenklach, *Combust. Flame* 110 (1997) 173–221.
- [41] A.D. Abid, N. Heinz, E. Tolmachoff, D. Phares, C. Campbell, H. Wang, *Combust. Flame* 154 (2008) 775–788.
- [42] A.D. Abid, E.D. Tolmachoff, D.J. Phares, H. Wang, Y. Liu, A. Laskin, *Proc. Combust. Inst.* 32 (2009) 681–688.
- [43] Z.G. Li, H. Wang, *Phys. Rev. E* 68 (2003) article 061206.
- [44] Z.G. Li, H. Wang, *Phys. Rev. E* 68 (2003) article 061207.
- [45] J. Singh, R.I.A. Patterson, M. Kraft, H. Wang, *Combust. Flame* 145 (2006) 117–127.
- [46] R.J. Kee, J.A. Miller, G.H. Evans, G. Dixon-Lewis, *Symp. (Int.) Combust.* 22 (1989) 1479–1494.
- [47] P.S. Veloo, 2010 Spring Technical Meeting, Western States Section of the Combustion Institute, University of Colorado, Boulder, CO, 2010, Paper 10S-19.
- [48] R.C. Peterson, N.M. Laurendeau, *Combust. Flame* 60 (1985) 279–284.
- [49] C.R. Shaddix, Proceedings of the 33rd National Heat Transfer Conference, Albuquerque, NM, 1999, Paper HTD99-282.